

**Effects of Geometrical Isomerism on Emissive Behaviour of
Heteroleptic Cyclometalated Ir(III) Complexes**

Journal:	<i>Dalton Transactions</i>
Manuscript ID	DT-ART-03-2021-000783.R2
Article Type:	Paper
Date Submitted by the Author:	02-May-2021
Complete List of Authors:	Jinsenji, Yoshiki ; Ehime University, Graduate School of Science and Engineering Takimoto, Kazuyoshi; Ehime University, Graduate School of Science and Engineering Yoshida, Jun; Kitasato University, chemistry Mori, Shigeki; Ehime University, Advanced Research Support Center Watanabe, Yutaka; Ehime University Sato, Hisako; Ehime University, Graduate School of Science and Engineering

ARTICLE

Effects of Geometrical Isomerism on Emissive Behaviour of Heteroleptic Cyclometalated Ir(III) Complexes

Yoshiki Jinsenji,^a Kazuyoshi Takimoto,^a Jun Yoshida,^b Shigeki Mori,^c Yutaka Watanabe,^a and Hisako Sato*^a

Received 00th January 20xx,
Accepted 00th January 20xx

DOI: 10.1039/x0xx00000x

In this study, we report the emissive properties of a heteroleptic cyclometalated Ir(III) complex, [Ir(bzq)₂(PBO)] (bzqH = benzo[h]quinoline; PBOH = 2-(2-hydroxyphenyl)benzoxazole). The complex, [Ir(C[^]N)₂(N[^]O)], was synthesised and optically resolved using a chiral column. Two geometrical isomers, *trans*-(N,N) and *cis*-(N,N) isomers, were obtained as the major and minor products in an enantiopure form, respectively. Their molecular structures were determined using single crystal X-ray analysis. In the crystalline states, the intermolecular C–H...π interaction between PBO[−] and an H atom in bzq[−] was the main factor influencing molecular packing. When the complexes were dissolved in CH₂Cl₂ and excited at 430 nm under N₂ atmosphere, yellow (λ_{max} = 550 nm) and orange emissions (λ_{max} = 570 nm) were observed for the *trans*-(N,N) and *cis*-(N,N) isomers, respectively, with the quantum yield higher for the former than the latter.

Introduction

Cyclometalated Ir(III) complexes are now attracting extensive attention as emitting elements in photoresponsive devices, such as sensors, electroluminescent (EL) devices, and photosensitisers.^{1–2} They are highly emissive in the visible region. In addition to these advantages as light emitters, they possess interesting structural character, such as *mer/fac* (*meridional/facial*) geometrical isomers together with ΔΔ coordination chirality.^{2–16} If this isomerism is combined with emissive properties, it may result in a multifunctional device based on Ir(III) complexes.^{17–29} In case of Ir(ppy)₃ (ppy = 2-phenylpyridyl), for example, the *mer* and *fac* isomers exhibit emission at 512 nm or 510 nm, respectively.⁵ The *fac* isomer gives quantum efficiency higher than the *mer* isomer. As another example, the photophysical properties of an Ir(III) complex containing two carbene-based ligands are reported to depend remarkably on *cis/trans* isomerism.³ Regarding chiral properties, we have studied the stereoselective effects on the emission behaviour of a chiral Ir(III) complex under asymmetric environments.²¹ Chiral photo-sensing was achieved using thin films based on these complexes.¹⁹

In this study, we synthesised a heteroleptic complex, [Ir(bzq)₂(PBO)] (bzqH = benzo[h]quinoline; PBOH = 2-(2-hydroxyphenyl)benzoxazole). Regarding the 2 ligands (C[^]N), the molecule is classified as [Ir(C[^]N)₂(N[^]O)], with 3 possible geometric isomers, *trans*-(N,N), *cis*-(N,N) and *trans*-(C,C), as shown in Chart 1. PBO[−] is characterised by its protonation and emission properties.³⁰ As a previous example, an Ir(III) complex containing PBO[−], *trans*-(N,N)-[Ir(ppy)₂(PBO)] was synthesised.³¹ Notably, in the present work, [Ir(bzq)₂(PBO)] was obtained as a mixture of *trans*-(N,N) and *cis*-(N,N) isomers as the major and minor products, respectively. Their structures were determined using single crystal X-ray diffraction. The effects of geometrical isomerism on emission behaviour were observed. To the best of our knowledge, this was the first report on the effects of geometrical isomerism on emissive behaviours for the complexes of [Ir(C[^]N)₂(N[^]O)] type.

Results and discussion

Synthetic procedure: The synthesis is described in the experimental section. The product of the reaction between [Ir(bzq)₂Cl]₂ and PBOH was eluted using a flash silica gel column (Experimental section). Chart 1 shows the molecular structures of the Ir(III) complexes used. The fraction containing the metal complexes was further eluted using an HPLC (High Performance Liquid Chromatography) silica gel column to separate the 2 main compounds represented by the peaks (Figure S1). These compounds were analysed using ¹H NMR, ¹³C NMR, single crystal X-ray diffraction, mass spectrometry, and elemental analysis (Figures S2–S5). Hence, the *trans*-(N,N) and *cis*-(N,N) isomers were identified as the major and minor products, respectively.

^a Graduate School of Science and Engineering, Ehime University, Matsuyama 790-8577, Japan, sato.hisako.my@ehime-u.ac.jp

^b Department of Chemistry, Kitasato University, Sagami-hara 252-0329, Japan

^c Advanced Research Support Center, Ehime University, Matsuyama 790-8577, Japan

Electronic Supplementary Information (ESI) available: chromatographic separation of *cis*-(N,N) and *trans*-(N,N) isomers of [Ir(bzq)₂(PBO)]; ¹H NMR, ¹³C NMR, MS data and elemental analyses; optical resolution of [Ir(bzq)₂(PBO)] isomers; electronic circular dichroism spectra of enantiomeric isomers of [Ir(bzq)₂(PBO)]; single crystal X-ray analyses of racemic and enantiomeric isomers of [Ir(bzq)₂(PBO)]; thermal isomerization of *trans*-(N,N)-[Ir(bzq)₂Cl]₂; emission properties of [Ir(bzq)₂(PBO)] under various conditions; theoretical calculations of [Ir(bzq)₂(PBO)] energy diagrams.

See DOI: 10.1039/x0xx00000x

When a racemic mixture of *trans*-(N,N)- and *cis*-(N,N)-[Ir(bzq)₂(PBO)] was eluted using a chiral HPLC column, 2 well-separated peaks with equal areas were obtained (Experimental section). A typical chromatogram is shown in the Figure S6. As shown later by their electronic circular dichroism (ECD) spectra, these peaks correspond to a pair of optical antipodes (Figure S7).

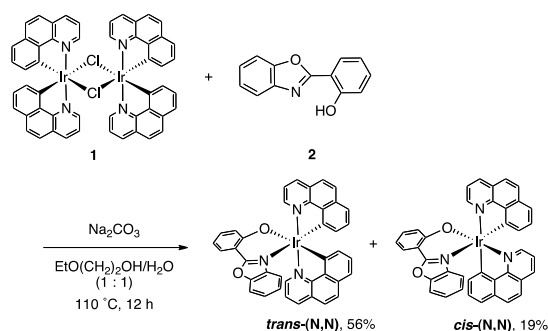


Chart 1. Isolation of geometric isomers, *trans*-(N,N)- and *cis*-(N,N)-[Ir(bzq)₂(PBO)]. Both products are racemic and expressed by one enantiomers.

Crystal structures of *cis*-(N,N) and *trans*-(N,N) isomers of [Ir(bzq)₂(PBO)]:

For the *cis*-(N,N)- and *trans*-(N,N)-[Ir(bzq)₂(PBO)] isomers, orange and yellow crystals, respectively, were obtained after slow evaporation of a CH₂Cl₂:hexane (1:3 v/v) solution. Single crystal X-ray structural analyses were performed on both the racemic and enantiomeric single crystals. The absolute configuration was determined for all investigated enantiomers.

The packing diagrams of racemic *cis*-(N,N)-[Ir(bzq)₂(PBO)], viewed along the *a*-, *b*-, and *c*-axes, are shown in Figures 1(a), 1(b), and 1(c), respectively. The space group is *P*-1. The molecular structure corresponds to the *cis*-(N,N) isomer (Chart 1). The molecules pack mainly through intermolecular $\pi \cdots \pi$ interactions. A pair of $\Delta\Lambda$ isomers form a loose association, with an Ir-Ir interatomic distance of 0.89 nm. Figure 2 shows the crystal structure of racemic *trans*-(N,N)-[Ir(bzq)₂(PBO)]. The space group is *P*-1 (details are available in the ESI†). Intermolecular C-H \cdots π interactions play a main role in the molecular packing. Therefore, a racemic pair forms a tight association, with an Ir-Ir interatomic distance of 0.68 nm, which is much smaller than the corresponding distance for a racemic pair of *cis*-(N,N) isomers (0.89 nm). The crystal structures of Δ -*cis*-(N,N)-[Ir(bzq)₂(PBO)] and Λ -*trans*-(N,N)-[Ir(bzq)₂(PBO)] are shown in Figures S8 and S9. The first and second peaks in the chromatogram were assigned to the Λ - and Δ -enantiomers, respectively. Interestingly, the enantiomers of the *cis*-(N,N) and *trans*-(N,N) isomers eluted in the opposite order using this chiral column. Table 1 compares the molecular and crystal structures of the *cis*-(N,N) and *trans*-(N,N) isomers. The detail crystallographic data including the selected bond distances and angles are shown

in the supporting information (Tables S1-S7 and Figures S10-14).

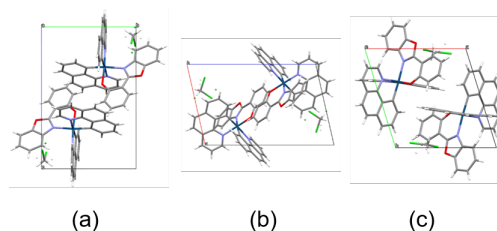


Figure 1 Racemic *cis*-(N,N)-[Ir(bzq)₂(PBO)] viewed along the (a) *a*-, (b) *b*-, and (c) *c*-axis, respectively. Solvent molecules are omitted for clarity. bzqH = benzo[h]quinoline; PBOH = 2-(2-hydroxyphenyl)benzoxazole.

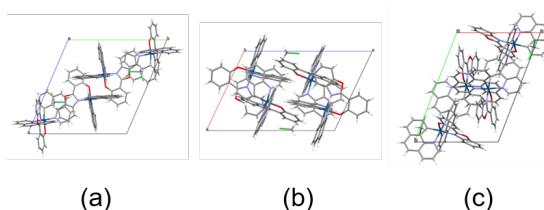


Figure 2 Racemic *trans*-(N,N)-[Ir(bzq)₂(PBO)] viewed along the (a) *a*-, (b) *b*-, and (c) *c*-axis, respectively. Solvent molecules are omitted for clarity. bzqH = benzo[h]quinoline; PBOH = 2-(2-hydroxyphenyl)benzoxazole.

Table 1. Summary of molecular interactions obtained using single crystal X-ray diffraction

	bzq-bzq	bzq-PBO	PBO-PBO	<i>d</i> _{Ir-Ir} /nm
Racemic <i>cis</i> -(N,N)	$\pi \cdots \pi$	C-H \cdots π	$\pi \cdots \pi$	0.89
Chiral <i>cis</i> -(N,N)	C-H \cdots π	$\pi \cdots \pi$	$\pi \cdots \pi$	0.89
Racemic <i>trans</i> -(N,N)	C-H \cdots π	C-H \cdots π	$\pi \cdots \pi$	0.68
Chiral <i>trans</i> -(N,N)	$\pi \cdots \pi$	C-H \cdots π	C-H \cdots π	0.92

Explanation for *cis*-(N,N)-[Ir(bzq)₂(PBO)] production:

In this study, both *cis*-(N,N) and *trans*-(N,N) isomers of [Ir(bzq)₂(PBO)] were produced as the minor and major products, respectively. This was unexpected due to the common view that the reaction of [Ir(C^{*N*})₂Cl]₂ with *trans*-(N,N) stereochemistry, with a bidentate ligand (L), yields *trans*-(N,N)-[Ir(C^{*N*})₂L] exclusively.³² To clarify at which step the configurational change took place, i.e., before or after cyclometalation, the dimer and *trans*-(N,N) were separately heated under conditions similar to the synthesis of [Ir(bzq)₂(PBO)]. The experiment using the dimer **1** gave 45% of dimeric mixtures, which included largely the starting stereoisomer **1** along with two minor isomers (Figure S15).

The residual products were too complex to isolate and identify. Although structural elucidation of the dimeric mixture was restricted due to the complex spectrum of the mixture, the high-resolution ESI (Electrospray Ionization) mass spectrum indicated a mixture of isomers with the same molecular formula and mass numbers due only to $[M-Cl]^+$ (Figure S16). In contrast, the *trans*-(N,N) isomer was intact without isomerisation. Therefore, *cis*-(N,N)-[Ir(bzq)₂(PBO)] may have been formed by PBOH ligation to an isomerisation product of the dimer $[Ir(bzq)_2Cl]_2$ with the *trans*-(N,N) configuration.

UV-vis and ECD spectra of the *cis*-(N,N) and *trans*-(N,N) isomers of [Ir(bzq)₂(PBO)]: Figure 3 shows the UV-vis (ultra violet-visible) spectra of the *cis*-(N,N) and *trans*-(N,N) isomers of [Ir(bzq)₂(PBO)] in CH₂Cl₂. For both isomers, the low-energy absorption band extending from 340 nm to the visible region is assigned to the ³MLCT and ³LLCT bands, while the dominant absorption band in the UV region, between 200 and 350 nm, is assigned to the π - π^* transition within the ligands. The ECD spectra of the resolved enantiomers in CH₂Cl₂ are shown in Figure S7. The mirror-image relationship is maintained between the antipodal pairs. The ³MLCT and ³LLCT bands show little ECD activity, whereas the π - π^* transition yields large ECD absorption peaks.

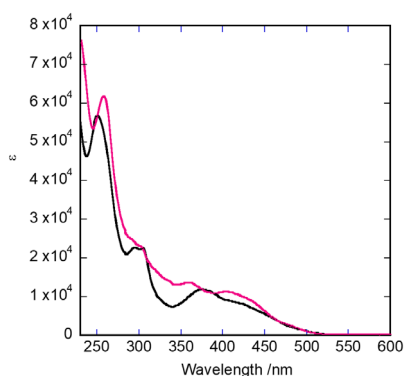


Figure 3. UV-vis spectra of (black) *cis*-(N,N)- and (red) *trans*-(N,N)-[Ir(bzq)₂(PBO)] in CH₂Cl₂. bzqH = benzo[h]quinoline; PBOH = 2-(2-hydroxyphenyl)benzoxazole.

The absolute configurations of these enantiomers were determined by single crystal X-ray analyses of the resolved species, as stated above.

Emission properties of the [Ir(bzq)₂(PBO)] isomers: The emission spectra of the Δ -*cis*-(N,N) and Δ -*trans*-(N,N) isomers of [Ir(bzq)₂(PBO)] were measured in CH₂Cl₂ under N₂ atmosphere. Figure 4 shows the spectra in the temperature range 253–293 K when the solutions were excited at 430 nm. The emission intensity increases with decreasing temperature. The peak wavelength (λ_{max}) and quantum yield

(Q.Y.) of the emissions are summarised in Table 2. The value of λ_{max} is 570 (orange) and 550 nm (yellow) at room temperature (20 °C) for the *cis*-(N,N) and *trans*-(N,N) isomers, respectively. Thus, the geometrical isomerism causes a difference of ca. 20 nm in the peak emission wavelength. The emissions under air and N₂ at room temperature are shown in Figure S17.

Emission decay was measured at room temperature by excitation with a light pulse at 355 nm. Examples of the obtained signals are shown in Figure 5. Decay curves were analysed using the following equation:

$$y = F_0 + F_1 \exp(-t/\tau), \quad (1)$$

where y is intensity count, τ is the relaxation time, t is time, F_1 is the emission amplitude, and F_0 is the emission background. The Q.Y. value was obtained independently, using $[Ru(bpy)_3]^{2+}$ as a reference. According to the literature, its Q.Y. is 0.028.³³ Using the observed values for τ and Q.Y. (denoted by ϕ), the non-radiative rate constant (k_{nr}) and radiative rate constant (k_r) were calculated using the following equations:^{34–36}

$$\phi = \frac{k_r}{k_r + k_{nr}}, \quad (2)$$

$$\tau = \frac{1}{k_r + k_{nr}}. \quad (3)$$

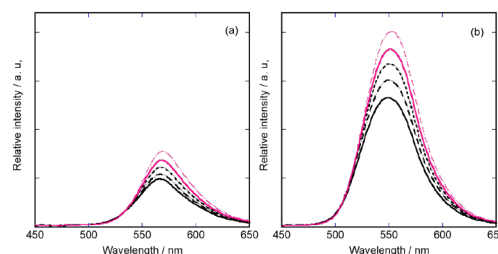


Figure 4. Emission spectra of (a) Δ -*cis*-(N,N)- and (b) Δ -*trans*-(N,N)-[Ir(bzq)₂(PBO)]. The complexes were dissolved at 5.4×10^{-5} M in CH₂Cl₂. The excitation wavelength is 430 nm. The bold black, broken black, dotted black, red bold and broken red lines correspond to 293, 283, 273, 263, and 253 K, respectively. bzqH = benzo[h]quinoline; PBOH = 2-(2-hydroxyphenyl)benzoxazole.

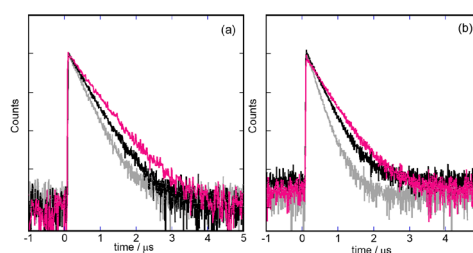


Figure 5. Decay curves of (a) Δ -*cis*-(N,N)- and (b) Δ -*trans*-(N,N)-[Ir(bzq)₂(PBO)]. The complexes were dissolved at 5.5×10^{-5} M in CH₂Cl₂. The excitation wavelength was 355 nm. The grey, black, and red curves were recorded at 293,

273, and 253 K, respectively. bzqH = benzo[h]quinoline; PBOH = 2-(2-hydroxyphenyl)benzoxazole.

The emission lifetime was in the sub-microsecond range, implying that the emission was phosphorescence. Comparing the kinetic results between the isomers, the *trans*-(N,N) isomer exhibited a higher Q.Y. despite its shorter lifetime. When the temperature was lowered, k_r remained almost constant, whereas k_{nr} decreased with decreasing temperature. Using the following equation,

$$k_{nr}(T) = k_a e^{-\Delta E/RT} \quad (4)$$

the activation energy (ΔE) for the rate constant of the non-radiative decay was 10.5 and 12.5 kJ mol⁻¹ for the *cis*-(N,N) and *trans*-(N,N) isomers, respectively. k_a denotes the rate constant of decay at infinite temperature. The obtained dynamic emission parameters are listed in Table 2.

Table 2. Dynamic emission parameters at 293 K, including quantum yield (ϕ), lifetime (τ), radiative rate constant (k_r), non-radiative rate constant (k_{nr}), and activation energy (ΔE).

	ϕ	τ / μ s	k_r /s ⁻¹	k_{nr} /s ⁻¹	ΔE /kJ mol ⁻¹
<i>cis</i> -(N,N)	0.22	0.47	4.63×10^5	1.64×10^6	10.5
<i>trans</i> -(N,N)	0.41	0.34	1.19×10^6	1.71×10^6	12.5

Theoretical estimation on stability of geometrical isomers:

The ground and excited states of [Ir(bzq)₂(PBO)] isomers were calculated using the Gaussian 16 program.³⁷ Upon comparison of the results of the theoretical calculations with the experimental observations, the following were noted. First, the total electronic energy of the ground state for the *trans*-(N,N) isomer is 16.9 kJ mol⁻¹ lower than that of the *cis*-(N,N) isomer, corresponding well to the higher amount of *trans*-(N,N) isomer obtained than *cis*-(N,N) isomer. Second, based on the ground state calculation, the energy gap between HOMO (highest occupied molecular orbital) and LUMO (lowest unoccupied molecular orbital) (denoted by $\Delta E_{\text{HOMO/LUMO}}$) is 3.67 (338 nm) and 3.73 eV (332 nm) for the *cis*-(N,N) and *trans*-(N,N) isomers, respectively (Figure S18). From the molecular orbital shapes of HOMO-1, HOMO, LUMO, LUMO+1, and LUMO+2, as shown in Figure S18, it was concluded that the main contributions to HOMO and LUMO came from the orbitals localized in PBO- and bzq- ligands, respectively. Based on the optimised triplet state geometries at the ground state, the phosphorescent emissive wavelengths are estimated from the transition energy (denoted by ΔSCF) between the ground singlet state (S_0) and the lowest triplet state (T_1). ΔSCF was calculated to be 2.38 eV (521 nm) and 2.42 eV (512 nm) for the *cis*-(N,N) and *trans*-(N,N) isomers, respectively. Experimentally, the peak positions of the main emission band were observed at 2.17 eV (570 nm) and 2.25 eV (550 nm) for the *cis*-(N,N) and *trans*-(N,N) isomers, respectively. Thus the theory predicted correctly the energy difference between these geometrical isomers.

(N,N) isomers, respectively. Thus the theory predicted correctly the energy difference between these geometrical isomers.

Experimental

Synthesis of [Ir(bzq)₂(PBO)]: A mixture of [Ir(bzq)₂Cl]₂ **1**^{31,32} (76.6 mg, 0.066 mmol), Na₂CO₃ (49.0 mg, 0.46 mmol) and PBOH **2** (36.5 mg, 0.17 mmol) in 2-ethoxyethanol:water (1:1, 12 mL) was stirred at 110 °C for 12 h under N₂. The reaction mixture was subjected to a flash silica gel column chromatography (eluent: CH₂Cl₂ containing 0.01 % CH₃OH) followed by purification by means of a silica gel column (GL Sciences, Japan) HPLC [eluent: CH₂Cl₂ (containing 0.01 % CH₃OH):hexane (10:1)] to give *cis*-(N,N) (19%) and *trans*-(N,N) (56%) (see ESI[†]).

Enantiomeric separation: The racemic Ir(III) complex was optically resolved using a chiral column (CHIRALPAK IC, Daicel Corp., Japan) with CH₂Cl₂ as the eluent at a flow rate of 0.5 mL min⁻¹, with the elution monitored at 350 nm. The HPLC results for the *cis*-(N,N) and *trans*-(N,N) isomers are shown in the ESI[†].

Instrumentation: NMR spectra were obtained using an AVIII 500 spectrometer (Bruker, Billerica, MA, USA) and JNM-AL400 (JEOL Ltd., Tokyo, Japan). UV-vis spectra were recorded using a V-730 UV-vis spectrophotometer (JASCO Co., Japan). Circular dichroism spectra were measured using a J-720 spectropolarimeter (JASCO Co., Japan). Emission spectra were recorded using an FP-6500 spectrofluorometer (JASCO Co., Japan) equipped with a cryostat (Unispeks, UNISOKU Co., Ltd., Osaka, Japan).

The emission lifetime was measured using a TSP-1000M-PL-ES (UNISOKU Co., Ltd., Osaka, Japan) equipped with a cryostat (Unispeks, UNISOKU Co., Ltd., Osaka, Japan). The instrument was also equipped with a pulsed YAG (Yttrium Aluminum Garnet) laser at 355 nm. The emission decay curve was obtained by averaging 130 pulsed signals. The curves were analysed under the assumption of single-exponential decay.

X-ray crystallography: X-ray diffraction was performed using a VariMax (Rigaku, Tokyo, Japan) with a Saturn diffractometer using multilayer mirror monochromated Mo K α ($\lambda = 0.71075$ Å) radiation at 100 \pm 1 K. Crystals were mounted on cryoloops. Collection of the reflection intensities and determination of the cell parameters were performed using CrystalClear 1.4.0 (Rigaku, Tokyo, Japan)⁴⁰ and CrysAlisPro 1.171.39.46 (Rigaku Oxford Diffraction).⁴¹ The data were corrected for Lorentz polarisation and absorption effects. The structures were solved using SHELXT-2018/2⁴² and expanded using the Fourier technique. All calculations were performed using the Olex2 1.2.⁴³ crystallographic software package, and SHELXL-2018/3⁴⁰ was used for structure refinement. The data were validated using PLATON.⁴⁴

Single crystals of racemic *cis*-(N,N)- and *trans*-(N,N)-[Ir(bzq)₂(PBO)] were prepared by slow evaporation of a CH₂Cl₂:hexane (1:3 v/v) solution. Crystallographic data:

Racemic *cis*-(N,N)-[Ir(bzq)₂(PBO)]; C₃₉H₂₄IrN₃O₂ and CH₂Cl₂, FW 843.74, triclinic, *P*-1, *a* = 10.4642(3) Å, *b* = 10.5088(2) Å, *c* = 15.5137(4) Å, α = 85.981(2)°, β = 76.654(2)°, γ = 72.389(2)°, *V* = 1582.12(7) Å³, *Z* = 2, μ = 4.432 mm⁻¹. *R*₁ = 0.0315 (*I* > 2 σ (*I*)), *wR*₂ = 0.0752 (all data), GOF = 1.051 (*I* > 2 σ (*I*)) (CCDC 2063612). Racemic *trans*-(N,N)-[Ir(bzq)₂(PBO)]; C₃₉H₂₄IrN₃O₂ and CH₂Cl₂, FW 843.74, triclinic, *P*-1, *a* = 12.2740(2) Å, *b* = 16.9938(3) Å, *c* = 18.1515(5) Å, α = 106.596(2)°, β = 109.535(2)°, γ = 103.187(2)°, *V* = 3192.42(13) Å³, *Z* = 4, μ = 4.392 mm⁻¹. *R*₁ = 0.0426 (*I* > 2 σ (*I*)), *wR*₂ = 0.0912 (all data), GOF = 1.022 (*I* > 2 σ (*I*)) (CCDC 2063615).

Computational details: Geometry optimization was performed at the DFT (density functional theory) level using the PBE0 functional. The basis set for Ir(III) was the (8s7p6d2f1g)/[6s5p3d2f1g] basis set combined with the Stuttgart quasi-relativistic ECP(effective core potential)^{37,38}, and the basis sets for the other atoms were the 6-31G(d,p) basis sets. All the calculations was performed using Gaussian 16 (C.01).³⁹ The solvent (CH₂Cl₂) was used in the polarisable continuum model approximation. The singlet and triplet ground states were optimised to calculate the Δ SCF. The optimized structures were confirmed to satisfy convergence conditions. At the optimized structures, all vibration had a positive sign and no negative frequency appeared.

Conclusion

The *trans*-(N,N) and *cis*-(N,N) isomers of a heteroleptic cyclometalated Ir(III) complex, [Ir(bzq)₂(PBO)], were obtained as the major and minor products, respectively. The production of the *cis*-(N,N) isomer is rare among similar synthetic approaches commencing from a corresponding dimeric species. Their molecular structures were determined using single crystal X-ray diffraction, and their emission properties in CH₂Cl₂ were investigated by altering the excitation wavelength and temperature. To the best of our knowledge, this is the first report on the influence of *cis-trans* isomerism on their emission behaviour of [Ir(C[^]N)₂(N[^]O)]-type Ir(III) complexes.

Conflicts of interest

There are no conflicts to declare.

Acknowledgements

This work was financially supported by the JSPS KAKENHI Grant-in-Aid for JP17H03044, JP19K05508, JP20K21090, and JST MIRAI grants (JPMJMI18GC). The computations were performed at the Research Center for Computational Science, Okazaki, Japan.

Notes and references

1. M. S. Lowry and S. Bernhard, *Chem. Eur. J.* 2006, **12**, 7970.
2. J. Lee, H.-F. Chen, T. Batagoda, C. Coburn, P. I. Djurovich, M. E. Thompson and S. R. Forrest, *Nat. Mater.*, 2016, **15**, 92.
3. F. Monti, M.G. I. L. Placa, N. Armaroli, R. Scopelliti, M. Gratzel, M. K. Nazeeruddin and F. Kessler, *Inorg. Chem.* 2015, **54**, 3031.
4. K. Dedeian, P. I. Djurovich, F. O. Garces, G. Carlson and R. J. Watts, *Inorg. Chem.* 1991, **30**, 1685.
5. A. B. Tamayo, B. D. Alleyne, P. I. Djurovich, S. Lamansky, I. Tsyba, N. N. Ho, R. Bau and M. E. Thompson, *J. Am. Chem. Soc.*, 2003, **125**, 7377.
6. K. Dedeian, J. Shi, N. Shepherd, E. Forsythe and D. C. Morton, *Inorg. Chem.*, 2005, **44**, 4445.
7. A. R. McDonald, M. Lutz, L. S. von Chrzanowski, G. P. M. van Klink, A. L. Spek and G. van Koten, *Inorg. Chem.*, 2008, **47**, 6681.
8. J. M. Fernández-Hernández, C.-H. Yang, J. I. Beltrán, V. Lemauro, F. Polo, R. Fröhlich, J. Cornil and L. D. Cola, *J. Am. Chem. Soc.*, 2011, **133**, 10543.
9. Y. Zheng, A. S. Batsanov, R. M. Edkins, A. Beeby and M. R. Bryce, *Inorg. Chem.* 2012, **51**, 290.
10. T. Setzer, C. Lennartz and A. Dreuw, *Dalton Trans.*, 2017, **46**, 7194.
11. Y. Tamura, Y. Hisamatsu, A. Kazama, K. Yoza, K. Sato, R. Kuroda and S. Aoki, *Inorg. Chem.*, 2018, **57**, 4571.
12. B.-S. Yun, J.-H. Kim, S.-Y. Kim, H.-J. Son, D. W. Cho and S. O. Kang, *Phys. Chem. Chem. Phys.*, 2019, **21**, 7155.
13. K. Tsuchiya, E. Ito, S. Yagai, A. Kitamura and T. Karatsu, *Eur. J. Inorg. Chem.*, 2009, 2104.
14. H. Huo, X. Shen, C. Wang, L. Zhang, P. Röse, L.-A. Chen, K. Harms, M. Marsch, G. Hilt and E. Meggers, *Nature*, 2014, **515**, 100; J. Ma, X. Zhang, X. Huang, S. Luo and E. Meggers, *Nature Protocols*, 2018, **13**, 605.
15. J. Otsuki, T. Tokimoto, Y. Noda, T. Yano, T. Hasegawa, X. Chen and Y. Okamoto, *Chem. Eur. J.* 2007, **13**, 2311.
16. M. Ashizawa, L. Yang, K. Kobayashi, H. Sato, A. Yamagishi, F. Okuda, T. Harada, R. Kuroda and M. Haga, *Dalton Trans.*, 2009, 1700.
17. G. Maseo, M. Fuseè, G. Longhi, I. Rimoldi, E. Cesarotti. A. Crispini and S. Abbate, *Dalton Trans.*, 2016, **45**, 992.
18. W. Guan, W. Zhou, J. Lu and C. Lu, *Chem. Soc. Rev.* 2015, **44**, 6981.
19. D. R. Martir, C. Momblona, A. Pertegás, D. B. Cordes, A. M. Z. Slawin, H. J. Bolink and E. Zysman-Colman, *ACS Appl. Mater. Interfaces*, 2016, **8**, 33907.
20. H. Sato, K. Tamura, M. Taniguchi and A. Yamagishi, *New J. Chem.*, 2010, **34**, 617.
21. K. Takimoto, Y. Watanabe, S. Mori and H. Sato, *Dalton Trans.* 2017, **46**, 4397; K. Takimoto, K. Tamura, Y. Watanabe, A. Yamagishi and H. Sato, *New J. Chem.* 2018, **42**, 4818.
22. P. A. Scattergood, A. M. Ranier, L. Charalambou, A. Comia, D. A. W. Ross, C. R. Rice, S. J. O. Hardman, J.-L. Heully, I. M. Dixon, M. Massi, F. Alary and P. I. P. Elliot, *Inorg. Chem.*, 2020, **59**, 1785.
23. H. Benjamin, Y. Zheng, V. N. Kozhevnikov, J. S. Siddle, L. J. O'Driscoll, M. A. Fox, A. S. Batsanov, G. C. Griffiths, F. B. Dias, A. P. Monkman and M. R. Bryce, *Dalton Trans.*, 2020, **49**, 2190.
24. A. Y. Gitlina, M. V. Ivonina, V. V. Sizov, G. L. Starova, A. P. Pushkarev, D. Volyniuk, S. P. Tunik, I. O. Koshevov and E. V. Grachova, *Dalton Trans.* 2018, **47**, 7578.
25. X.-Y. Liu, Y.-H. Zhang, W.-H. Fang and G. Cui, *J. Phys. Chem. A* 2018, **122**, 5518.

26. S. Kumar, Y. Hisamatsu, Y. Tamaki, O. Ishitani and S. Aoki, *Inorg. Chem.*, 2016, **55**, 3829.
27. E. Pomario, M. Silatani, F. Messina, O. Braem, A. Cannizzo, E. Barranoff, J. H. Klein, C. Lambert and M. Chergui, *J. Phys. Chem. C*, 2016, **120**, 16459.
28. S. Ladouceur, L. Donato, M. Romain, B. P. Mudraboynia, M. B. Johansen, J. A. Wisner and E. Zysman-Colman, *Dalton Trans.*, 2013, **42**, 8838.
29. S.-H. Wu, J.-W. Ling, S.-H. Lai, M.-J. Huang, C. H. Cheng and I.-C. Chen, *J. Phys. Chem. A*, 2010, **114**, 10339.
30. W.-H. Chen and Y. Pang, *Tetrahedron Lett.*, 2010, **51**, 1914.
31. Y. Liu, M. Li, Q. Zhao, H. Wu, K. Huang and F. Li, *Inorg. Chem.*, 2011, **50**, 5969.
32. M. Nonoyama, *Bull. Chem. Soc. Jpn.*, 1974, **47**, 767.
33. K. Nakamaru, *Bull. Chem. Soc. Jpn.*, 1982, **55**, 2697.
34. S. Koseki, N. Kamata, T. Asada, S. Yagi, H. Nakazumi and T. Matsushita, *J. Phys. Chem. C*, 2013, **117**, 5314.
35. X. Zhou, P. L. Burn and B. J. Powell, *Inorg. Chem.*, 2016, **55**, 5266.
36. X. Wang, H. Yang, Y. Wen, L. Wang, J. Li and J. Zhang, *Inorg. Chem.*, 2017, **56**, 8986.
37. D. Andrae, U. Haeussermann, M. Dolg, H. Stoll, H. Preuss, *Theor. Chim. Acta*, 1990, **77**, 123.
38. J. M. L. Martin, A. Sundermann, *J. Chem. Phys.*, 2001, **114**, 3408.
39. M. J. Frisch, G. W. Trucks, H. B. Schlegel, G. E. Scuseria, M. A. Robb, J. R. Cheeseman, G. Scalmani, V. Barone, G. A. Petersson, H. Nakatsuji, X. Li, M. Caricato, A. V. Marenich, J. Bloino, B. G. Janesko, R. Gomperts, B. Mennucci, H. P. Hratchian, J. V. Ortiz, A. F. Izmaylov, J. L. Sonnenberg, D. Williams-Young, F. Ding, F. Lipparini, F. Egidi, J. Goings, B. Peng, A. Petrone, T. Henderson, D. Ranasinghe, V. G. Zakrzewski, J. Gao, N. Rega, G. Zheng, W. Liang, M. Hada, M. Ehara, K. Toyota, R. Fukuda, J. Hasegawa, M. Ishida, T. Nakajima, Y. Honda, O. Kitao, H. Nakai, T. Vreven, K. Throssell, J. A. Montgomery, Jr., J. E. Peralta, F. Ogliaro, M. J. Bearpark, J. J. Heyd, E. N. Brothers, K. N. Kudin, V. N. Staroverov, T. A. Keith, R. Kobayashi, J. Normand, K. Raghavachari, A. P. Rendell, J. C. Burant, S. S. Iyengar, J. Tomasi, M. Cossi, J. M. Millam, M. Klene, C. Adamo, R. Cammi, J. W. Ochterski, R. L. Martin, K. Morokuma, O. Farkas, J. B. Foresman and D. J. Fox, Gaussian, Inc., Wallingford CT, 2019., GAUSSIAN 16 (Revision C.01), Gaussian, Inc. Wallingford, CT, 2019.
40. *CrystalClear, Data collection and processing software*, Rigaku Corporation, Japan, 2010.
41. *CrysAlisPro, Data collection and processing software*, Rigaku Corporation, Japan, 2018.
42. *SHELXL Version 2016/6*: G. M. Sheldrick, *Acta Crystallogr., Sect. C: Cryst. Struct. Commun.*, 2015, **71**, 3.
43. O. V. Dolomanov, L. J. Bourhis, R. J. Gildea, J. A. K. Howard and H. Puschmann, *J. Appl. Cryst.*, 2009, **42**, 339.
44. PLATON: A. L. Spek, *Acta Crystallogr., Sect. D: Biol. Crystallogr.*, 2009, **65**, 148.